https://doi.org/10.1016/j.engstruct.2021.112228

Analytical formulas of thermal deformation of suspension bridges

Yi ZHOU[a,b,*], Yong XIA[a,*], Yozo FUJINO[c], Kazunori YAMAGUCHI[d]

[a] Department of Civil and Environmental Engineering, The Hong Kong Polytechnic University, Hong Kong, China

[b] Beijing Key Laboratory of Urban Underground Space Engineering, University of Science & Technology Beijing, Beijing 100083, China

[c] Institute of Advanced Sciences, Yokohama National University, Yokohama 240-8501, Japan

[d] Honshu-Shikoku Bridge Expressway Co., Ltd., Kobe 651-0088, Japan

[*] Corresponding authors. E-mail: zhouyi@ustb.edu.cn (Y. Zhou), ceyxia@polyu.edu.hk (Y. Xia).

ABSTRACT Deformation of a long-span suspension bridge is mainly caused by ambient temperature changes. The temperature-induced deformation of a bridge is usually calculated using complex three-dimensional finite element analysis, the mechanism of which is often unclear. In this study, we derive general, succinct analytical formulas of the thermal deformation of three-span suspension bridges. The deformation of different components is unified into a one-dimensional thermal expansion formula ($\delta L = L_{\mathrm{E}}\theta \cdot \delta T$) by introducing an equivalent length L_{E}. The sag effect of side-span cables is characterized by the modification coefficients, which demonstrate that the neglect of the sag effect overestimates the thermal deformation. Furthermore, the thermal deformation of the main- and side-span cables and towers is found to interact with each other as a result of the cable tension changes with varying temperature. The analytical formulas are validated using eight long-span suspension bridges including the Akashi Kaikyo bridge, the longest main-span suspension bridge in the world. The closed-form solutions herein also apply to the self-anchored suspension bridges.

KEYWORDS Suspension bridge, thermal deformation, analytical solution, sag effect, structural health monitoring.

1 Introduction

Suspension bridges are a perfect combination of art, science, and technology because of their elegant appearance, long span, and high strength [1, 2]. Compared with other bridge types, suspension bridges exhibit the largest spanning capacity but the lowest global stiffness, and therefore their deformation under various loadings is a major concern [3-5]. With the development of the structural health monitoring technology, more and more civil structures have been equipped with comprehensive monitoring systems since the 1990s [6-8]. Field monitoring systems demonstrate that temperature variations dominate the quasi-static deformation of suspension bridges [9, 10]. For example, the mid-span elevation of the Akashi Kaikyo bridge of Japan exhibited a 2-m variation because of a change in yearly ambient temperature [11].

The temperature-induced deformation of suspension bridges has been analyzed using three approaches: regression techniques [9, 12, 13], finite element (FE) analyses [14-16], and analytical formulas [17, 18]. Regression techniques and FE analyses require a separate study for different bridges and are therefore hard to explain the mechanism of the thermal action on bridges. Moreover, regression techniques depend on measurement data and can only be used to determine statistical relations between temperature and deformation. FE analyses require numerous manual efforts in modeling. Their accuracy heavily depends on the operator's experience.

Analytical formulas own the advantages of clear concept, simple calculation, and general applicability. Most existing formulas in bridge engineering estimate deformation caused by live loads instead of temperature action [19-21]. For thermal deformation, a one-dimensional (1D) thermal expansion formula $\delta L_{\text{org}} = L_{\text{org}}\theta \cdot \delta T$ (where L_{org}, T, and θ represent the original free length, temperature, and linear expansion coefficient of the structural component, respectively, and $\delta(\cdot)$ denotes the quantity change) is commonly used to estimate the temperature-induced longitudinal displacement of girders and towers [22]. Timoshenko and Young [17] derived an algebraic formula to estimate the sag change in a horizontal single-span cable caused by changes in cable temperature. The aforementioned formula is too simple and cannot be used to calculate the deformation of complex suspension bridges. Recently, Zhou et al. [18] proposed analytical formulas to calculate the temperature-induced structural displacement of a ground-anchored suspension bridge. However, the derivation idealizes the side-span cables as straight anchor cables, which is impossible in practice and may lead to considerable errors for bridges with long side spans. Also, the deformations of the side- and main-span cables and towers are analysed separately and then summed up in Ref. [18] by using simplified geometric models, and the mutual influence between adjacent span cables and the temperature-induced cable tension changes are neglected.

In this study, a general methodology for calculating the global thermal deformation of the girders, towers, and main cables of three-span suspension bridges is proposed. The methodology treats a suspension bridge as an assembly of interconnected members, and considers the effects of the side-span cable sags and the cable tension changes with temperature. The resulting formulas have a unified simple form similar to 1D thermal expansion formula and provide clear physical interpretation of thermal deformation of suspension bridges.

2 Analytical formulation

Consider a common two-tower three-span ground-anchored suspension bridge [Fig. 1(a)]. The main cable is divided into three spans of l_i (i = 1, 2, and 3 represent the left side-span, main-span, and right side-span cables, respectively) by the two upright towers with a height of $h_{\text{p}i}$ ($i = 1, 2$). The two tower tops, which act as the intermediate supports to the main cable, are not necessarily located at the same level. The sag and cable-chord inclination of each span cable are denoted as f_i and α_i ($i = 1, 2, 3$), respectively, where f_i is a positive value measured downward from the midpoint of the cable chord, and α_i is positive for the counter clockwise rotation from the horizontal. Note that f_i is referred to the midpoint rather than the lowest point of the cable, and a suspension bridge always has $\alpha_1 > 0$ and $\alpha_3 < 0$ for the calculation convenience. For each span cable, the elevation difference between the two end supports is $h_i = l_i \tan\alpha_i$ ($i = 1, 2, 3$). The total horizontal distance between the two anchorages is $L = \sum_{i=1}^{3} l_i$.

The deformed configuration of the bridge is illustrated in Fig. 1(b) when main cables and bridge towers experience a uniform temperature variation. The following assumptions, justified in Appendix A, are adopted in the bridge deformation analysis:

(1) The cable curve between two consecutive supports is a parabola, and its length varies because of temperature changes only.

(2) The horizontal tensions of main cables on both sides of a tower top are always equal.

(3) The stiffening girder and suspenders do not prevent movement of the main cable.

(4) The main cables are firmly fixed to the anchorages and tower tops.

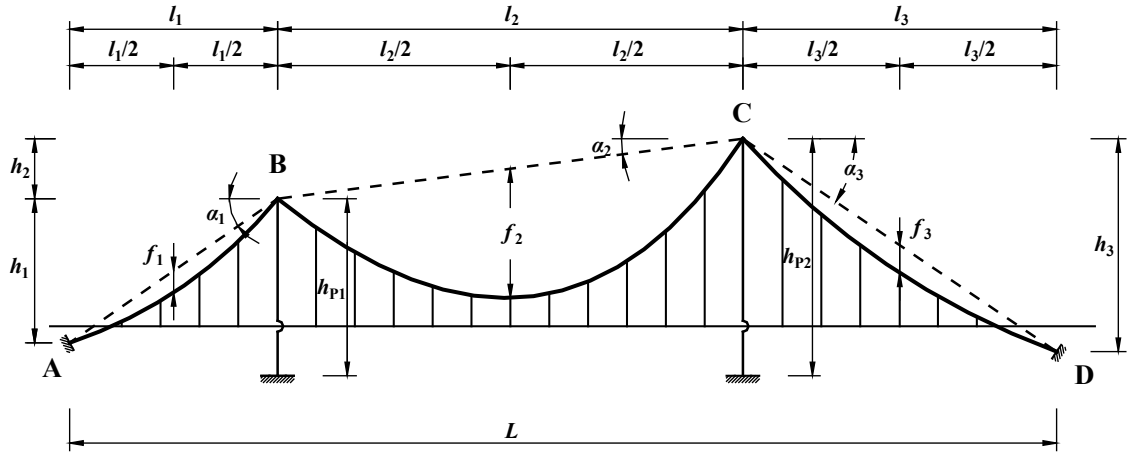

(a) Structural configuration.

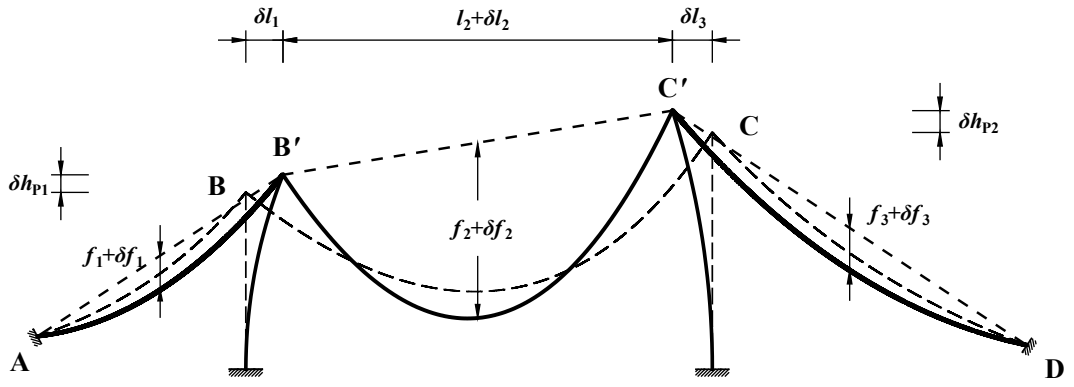

(b) Structural deformation.

Fig. 1. Analytical model of a general two-tower ground-anchored suspension bridge.

The sag of the i^{th} cable can be expressed as [1, 18]:

$$f_i = \frac{q_i l_i^2}{8H_i} = \frac{W_i l_i}{8H_i} \tag{1}$$

where q_i is the uniformly distributed vertical load, H_i is the horizontal component of the tension force, and $W_i = q_i l_i$ is the total vertical load acting on the cable. Because $\delta W_i = 0$, the differentiation of Eq. (1) produces

$$\frac{\delta f_i}{f_i} = \frac{\delta l_i}{l_i} - \frac{\delta H_i}{H_i} \tag{2}$$

A horizontal force equilibrium at the tower top is always maintained (that is, $H_1 = H_2 = H_3$ and $\delta H_1 = \delta H_2 = \delta H_3$); thus, we acquire the following equations for $i = 1, 2$:

$$\frac{\delta f_i}{f_i} - \frac{\delta f_{i+1}}{f_{i+1}} = \frac{\delta l_i}{l_i} - \frac{\delta l_{i+1}}{l_{i+1}} \tag{3}$$

The cable length S_i ($i = 1, 2, 3$) is [18]

$$S_i = l_i \left(\sec\alpha_i + \frac{8}{3} n_i^2 \cos^3 \alpha_i \right) \tag{4}$$

where $n_i = f_i / l_i$ is the sag-to-span ratio.

Differentiating Eq. (4) yields

$$\delta S_i = c_{ni} \cdot \delta n_i + c_{li} \cdot \delta l_i + c_{\alpha i} \cdot \delta\alpha_i \tag{5}$$

where the coefficients c_{ni}, c_{li}, and $c_{\alpha i}$ are

$$c_{ni} = \frac{\partial S_i}{\partial n_i} = \frac{16}{3} n_i l_i \cos^3 \alpha_i \tag{6}$$

$$c_{li} = \frac{\partial S_i}{\partial l_i} = \sec \alpha_i + \frac{8}{3} n_i^2 \cos^3 \alpha_i \tag{7}$$

$$c_{\alpha i} = \frac{\partial S_i}{\partial \alpha_i} = l_i \left(\frac{\sin \alpha_i}{\cos^2 \alpha_i} - 8 n_i^2 \sin \alpha_i \cos^2 \alpha_i \right) \tag{8}$$

Differentiating $n_i = f_i / l_i$ with respect to f_i and l_i provides

$$\delta n_i = \delta \left(\frac{f_i}{l_i} \right) = \frac{l_i \cdot \delta f_i - f_i \cdot \delta l_i}{l_i^2} \tag{9}$$

As $h_i = l_i \tan \alpha_i$ ($i = 1, 2, 3$), differentiating h_i with respect to l_i and α_i leads to $\delta h_i = \delta l_i \cdot \tan \alpha_i + l_i \sec^2 \alpha_i \cdot \delta \alpha_i$. Because δh_i is equal to the difference between the change in tower height, that is, $\delta h_i = \delta h_{\mathrm{P}i} - \delta h_{\mathrm{P}(i-1)}$, $\delta \alpha_i$ is obtained as

$$\delta \alpha_i = -\frac{\sin 2\alpha_i}{2 l_i} \cdot \delta l_i + \frac{\cos^2 \alpha_i}{l_i} \left(\delta h_{\mathrm{P}i} - \delta h_{\mathrm{P}(i-1)} \right) \tag{10}$$

where $\delta h_{\mathrm{P}0} = \delta h_{\mathrm{P}3} = 0$ because they correspond to unmovable anchorage blocks. Substituting Eqs. (9) and (10) into Eq. (5) yields the following equations ($i = 1, 2, 3$):

$$\frac{c_{ni}}{l_i} \cdot \delta f_i + M_i \cdot \delta l_i = Q_i \tag{11}$$

where

$$M_i = -\frac{c_{ni} n_i}{l_i} + c_{li} - \frac{c_{\alpha i} \sin 2\alpha_i}{2 l_i} \tag{12}$$

$$Q_i = \delta S_i - \frac{c_{\alpha i} \cos^2 \alpha_i}{l_i} \left(\delta h_{\mathrm{P}i} - \delta h_{\mathrm{P}(i-1)} \right) \tag{13}$$

Because the distance between the two anchorages is constant, the following is true:

$$\delta l_1 + \delta l_2 + \delta l_3 = 0 \tag{14}$$

Consequently, Eqs. (3), (11), and (14) constitute a set of linear equations of δf_i and δl_i ($i = 1, 2, 3$):

$$\left[\begin{array}{ccc:ccc} c_{n1} l_1^{-1} & 0 & 0 & M_1 & 0 & 0 \\ 0 & c_{n2} l_2^{-1} & 0 & 0 & M_2 & 0 \\ 0 & 0 & c_{n3} l_3^{-1} & 0 & 0 & M_3 \\ \hdashline -f_1^{-1} & f_2^{-1} & 0 & l_1^{-1} & -l_2^{-1} & 0 \\ 0 & -f_2^{-1} & f_3^{-1} & 0 & l_2^{-1} & -l_3^{-1} \\ 0 & 0 & 0 & 1 & 1 & 1 \end{array}\right] \cdot \left[\begin{array}{c} \delta f_1 \\ \delta f_2 \\ \delta f_3 \\ \hdashline \delta l_1 \\ \delta l_2 \\ \delta l_3 \end{array}\right] = \left[\begin{array}{c} Q_1 \\ Q_2 \\ Q_3 \\ \hdashline 0 \\ 0 \\ 0 \end{array}\right] \tag{15}$$

If the second order terms of n in c_{li} and $c_{\alpha i}$ ($i = 1, 2, 3$) are omitted, then Eq. (15) can be solved as (see Appendix B)

$$\delta f_i = \frac{n_i \cdot \delta S_i}{\cos \alpha_i} - n_i \tan \alpha_i \left(\delta h_{\mathrm{P}i} - \delta h_{\mathrm{P}(i-1)} \right) + \frac{n_i (l_i - z_i)}{\sum_{j=1}^{3} z_j} \sum_{j=1}^{3} \left[\frac{\delta S_j}{\cos \alpha_j} - \tan \alpha_j \left(\delta h_{\mathrm{P}j} - \delta h_{\mathrm{P}(j-1)} \right) \right] \tag{16}$$

$$\delta l_i = \frac{\delta S_i}{\cos \alpha_i} - \tan \alpha_i \left(\delta h_{\mathrm{P}i} - \delta h_{\mathrm{P}(i-1)} \right) - \frac{z_i}{\sum_{j=1}^{3} z_j} \sum_{j=1}^{3} \left[\frac{\delta S_j}{\cos \alpha_j} - \tan \alpha_j \left(\delta h_{\mathrm{P}j} - \delta h_{\mathrm{P}(j-1)} \right) \right] \tag{17}$$

where

$$z_i = \frac{16}{3} l_i n_i^2 \cos^2 \alpha_i \tag{18}$$

Eqs. (16) and (17) are the sag change of the main cables and horizontal displacement of the tower tops, respectively. Because main cables and towers are subjected to the temperature changes δT_{C} and δT_{P}, respectively, and θ_{C} and θ_{P} are the corresponding coefficients of linear expansion, we have

$$\delta S_i = S_i \theta_{\mathrm{C}} \cdot \delta T_{\mathrm{C}} = l_i \theta_{\mathrm{C}} \sec \alpha_i \cdot \delta T_{\mathrm{C}} \tag{19}$$

$$\delta h_{\mathrm{P}j} = h_{\mathrm{P}j} \theta_{\mathrm{P}} \cdot \delta T_{\mathrm{P}} \tag{20}$$

where δS_i ($i = 1, 2, 3$) and $\delta h_{\mathrm{P}j}$ ($j = 0, 1, 2, 3$) represent the contribution from the temperature change in cables and towers, respectively; and the second order term of n in S_i (Eq. (4)) is neglected.

The change in the mid-span elevation of the main-span cable is the sum of the sag and tower height changes. Let the upward movement be positive; thus, it has

$$\delta D_2 = -\delta f_2 + \frac{h_{\mathrm{P1}} + h_{\mathrm{P2}}}{2} \theta_{\mathrm{P}} \cdot \delta T_{\mathrm{P}} \tag{21}$$

Because the suspender at the mid-span is usually short, it undergoes negligible thermal deformation, and the main cable and the girder at the mid-span exhibit nearly the same vertical displacement δD_2.

Both anchorages are unmovable. δl_1 and δl_3 are thus equal to the tower-top horizontal displacement, which takes positive values when the tower top moves toward the central span. δl_2 corresponds to the variation in the horizontal distance of the tower tops.

3 Simplified formulas

Eqs. (16) and (17) are rather complicated. They are simplified in this section for practical bridges.

For side-span cables hanging with a girder, q_i of the side-span and main-span cables are considered identical. Eq. (1) can be rewritten as

$$n_i = \frac{f_i}{l_i} = \frac{q_i l_i}{8 H_i} \tag{22}$$

Then n_i is proportional to the span length l_i. Introducing a span ratio ζ_i into Eq. (22) yields

$$\zeta_i = \frac{l_i}{l_2} = \frac{n_i}{n_2} \tag{23}$$

For the main-span cable, $\zeta_2 = 1$, and for the side-span cable, ζ_i ($i = 1, 3$) is usually <0.5 and $n_i = \zeta_i n_2 \le 1/20$ ($i = 1, 3$) because $n_2 \approx 1/10$ [23].

From Eq. (18),

$$\frac{z_i}{l_i} = \frac{16 \cdot l_i n_i^2 \cos^2 \alpha_i}{3 l_i} = \frac{16}{3} n_2^2 \cdot \zeta_i^2 \cdot \cos^2 \alpha_i \le \frac{16}{3} n_2^2 \cdot \zeta_i^2 \approx \frac{4}{75} \zeta_i^2 \tag{24}$$

Consequently, $z_i / l_i \le 1.3\%$ ($i = 1$ and 3) and $z_2 / l_2 \le 5.3\%$. Therefore, $l_i - z_i \approx l_i$. This approximation is also feasible for side-span cables without suspenders. Substituting $l_i - z_i \approx l_i$, $\delta S_i = l_i \theta_{\mathrm{C}} \sec \alpha_i \cdot \delta T_{\mathrm{C}}$, $\sec \alpha_i = \sqrt{l_i^2 + h_i^2} / l_i$, $\tan \alpha_i = h_i / l_i$ ($i = 1, 2, 3$), and $\delta h_{\mathrm{P}j} = h_{\mathrm{P}j} \theta_{\mathrm{P}} \cdot \delta T_{\mathrm{P}}$ ($j = 0, 1, 2, 3$) into Eq. (16), we obtain the following:

$$\delta f_i = n_i \left[\frac{l_i^2 + h_i^2}{l_i} \theta_{\mathrm{C}} \cdot \delta T_{\mathrm{C}} - \frac{h_i \cdot \left(h_{\mathrm{P}i} - h_{\mathrm{P}(i-1)} \right)}{l_i} \theta_{\mathrm{P}} \cdot \delta T_{\mathrm{P}} \right] + \frac{l_i n_i}{\sum_{k=1}^{3} z_k} \sum_{j=1}^{3} \left[\frac{l_j^2 + h_j^2}{l_j} \theta_{\mathrm{C}} \cdot \delta T_{\mathrm{C}} - \frac{h_j \cdot \left(h_{\mathrm{P}j} - h_{\mathrm{P}(j-1)} \right)}{l_j} \theta_{\mathrm{P}} \cdot \delta T_{\mathrm{P}} \right] \tag{25}$$

For most suspension bridges, the following four approximations are applicable: (1) $h_{\mathrm{P1}} \approx h_1$, (2) $h_{\mathrm{P2}} \approx |h_3|$, (3) $\theta_{\mathrm{C}} \cdot \delta T_{\mathrm{C}} \approx \theta_{\mathrm{P}} \cdot \delta T_{\mathrm{P}}$, and (4) $h_{\mathrm{P2}} - h_{\mathrm{P1}} \approx h_2$ (both tower bottoms at the same level) or $h_2 = 0$ (both tower tops at the same level, or $\alpha_2 = 0$). Eq. (25) then becomes:

$$\delta f_i = n_i l_i \theta_C \cdot \delta T_C + \frac{n_i l_i}{\sum_{k=1}^{3} z_k} \theta_C \cdot \delta T_C \cdot \sum_{j=1}^{3} l_j \tag{26}$$

The ratio of the first to second items in Eq. (26) is

$$\frac{\sum_{i=1}^{3} z_i}{\sum_{i=1}^{3} l_i} = \frac{16 \cdot \sum_{i=1}^{3} l_i n_i^2 \cos^2 \alpha_i}{3 \cdot \sum_{i=1}^{3} l_i} \tag{27}$$

Because $n_2 \approx 1/10$, $n_i \le 1/20$ ($i = 1, 3$), Eq. (27) is considerably lower than 1. Therefore, the first item of Eq. (26) is negligible compared with the second item. Consequently, Eq. (16) can be simplified as follows

$$\delta f_i = \frac{f_i}{\sum_{j=1}^{3} z_j} L \theta_C \cdot \delta T_C \tag{28}$$

Similarly, Eq. (17) for the tower-top horizontal displacement δl_i ($i = 1, 2, 3$) can be simplified as

$$\delta l_i = \left(l_i - \frac{z_i}{\sum_{j=1}^{3} z_j} L \right) \theta_C \cdot \delta T_C \tag{29}$$

Eqs. (28) and (29) exhibit a unified form similar to 1D thermal deformation $L_E \theta_C \cdot \delta T_C$, where L_E is the temperature equivalent length and can be expressed as

$$L_E = \begin{cases} \dfrac{f_i}{\sum_{j=1}^{3} z_j} L & \text{for } \delta f_i, i = 1, 2, 3 \\ l_i - \dfrac{z_i}{\sum_{j=1}^{3} z_j} L & \text{for } \delta l_i, i = 1, 2, 3 \end{cases} \tag{30}$$

When the sags of both side-span cables are neglected, that is, $f_1 = f_3 = 0$, the temperature equivalent length can be simplified as

$$L_E = \begin{cases} 0 & \text{for } \delta f_1, \delta f_3 \\ 3L \big/ \left(16 n_2 \cos^2 \alpha_2\right) & \text{for } \delta f_2 \\ l_1 & \text{for } \delta l_1 \\ -\left(l_1 + l_3\right) & \text{for } \delta l_2 \\ l_3 & \text{for } \delta l_3 \end{cases} \tag{31}$$

When the main-span cable has a horizontal chord ($\alpha_2 = 0$), Eq. (31) is identical to the formula in Ref. [18]. Therefore, the present approach is more general than Ref. [18]. The sag effect of the side-span cables can be quantified by comparing the two temperature equivalent lengths in Eqs. (30) and (31), as presented in Section 5.

4 Verification of formulas

The Akashi Kaikyo bridge is used to verify the proposed formula. The bridge is a three-span suspension bridge across the Akashi Strait in Japan with a steel truss-stiffened girder and diagonally braced steel towers. It was opened to the public in April 1998, and since then has had the longest span of any bridge in the world [24].

A structural health monitoring system was installed on the bridge to measure various loadings such as wind, earthquake, traffic, and temperature and their effects. Fig. 2 shows the layout of the temperature sensors and GPS stations used in this study. The cable temperature was measured at three locations: near the anchorage 1A (T1), at the top of tower 2P (T2), and near the mid-span of the central span (T3). Moreover, a thermometer was installed near the midpoint of the central span girder (T4) to measure air temperature. Structural displacement was measured by using GPS with a reference station at the 1A anchorage and two rovers, namely one on the 2P tower top (GPS1) and the other

on the mid-span of the central span girder (GPS2).

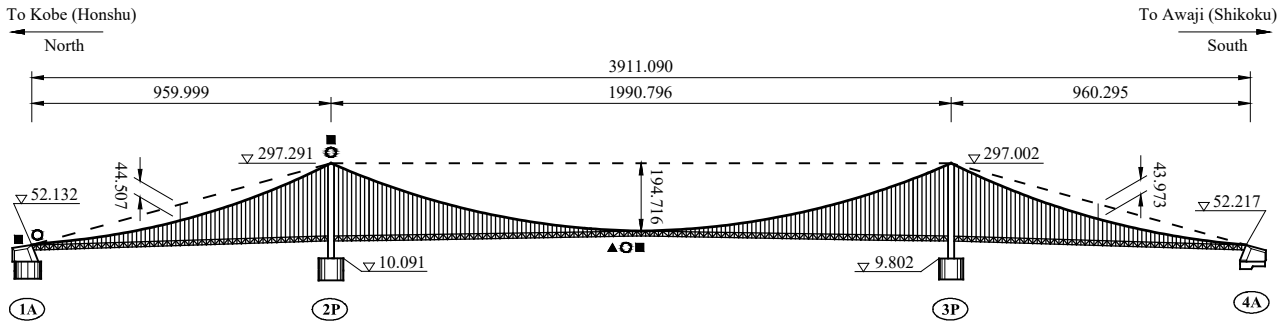

Fig. 2. Configuration of the Akashi Kaikyo bridge and GPS and temperature measurement points (Unit: m; ■: GPS station, ○: cable temperature sensor, ▲: air temperature sensor. The elevation is measured from the Tokyo Bay mean tide level).

The 10-min means of temperature and structural displacement obtained from September 1998 to August 2001 are studied. The averaging can filter out the high frequency components of the displacement due to dynamic loadings such as wind and traffic. Consequently the 10-min means represent the temperature-related structural response.

Fig. 3 presents the cable and air temperatures, the tower-top horizontal displacement of tower 2P, and the mid-span elevation of the main-span girder during the study period. The discontinuity of the curves in the figure is caused by malfunction of the monitoring equipment. With the temperature increase, the tower top moves toward the central span (approximately 20 cm in a year), and the midpoint of the main-span girder moves downward (approximately 200 cm), demonstrating that temperature change governs the global deformation of the bridge in the operational stage.

Additionally, Fig. 3 presents the temperature and displacement measured between July 7 and July 9, 1999. Cable temperatures T1 and T2 vary at the same magnitude and pace. Their daily variations are smaller than that of the cable temperature T3. Moreover, T1 and T2 lag behind T3 and air temperature T4 by approximately 7 h. This is because T1 and T2 sensors were installed inside the main cables (underneath the polyethylene tubes) whereas T3 thermometer was attached to the cable band. The latter is affected by air temperature and solar radiation. Because the resolution of GPS data was relatively low 20 years ago, the small swaying movement of the tower exhibits a stepped shape.

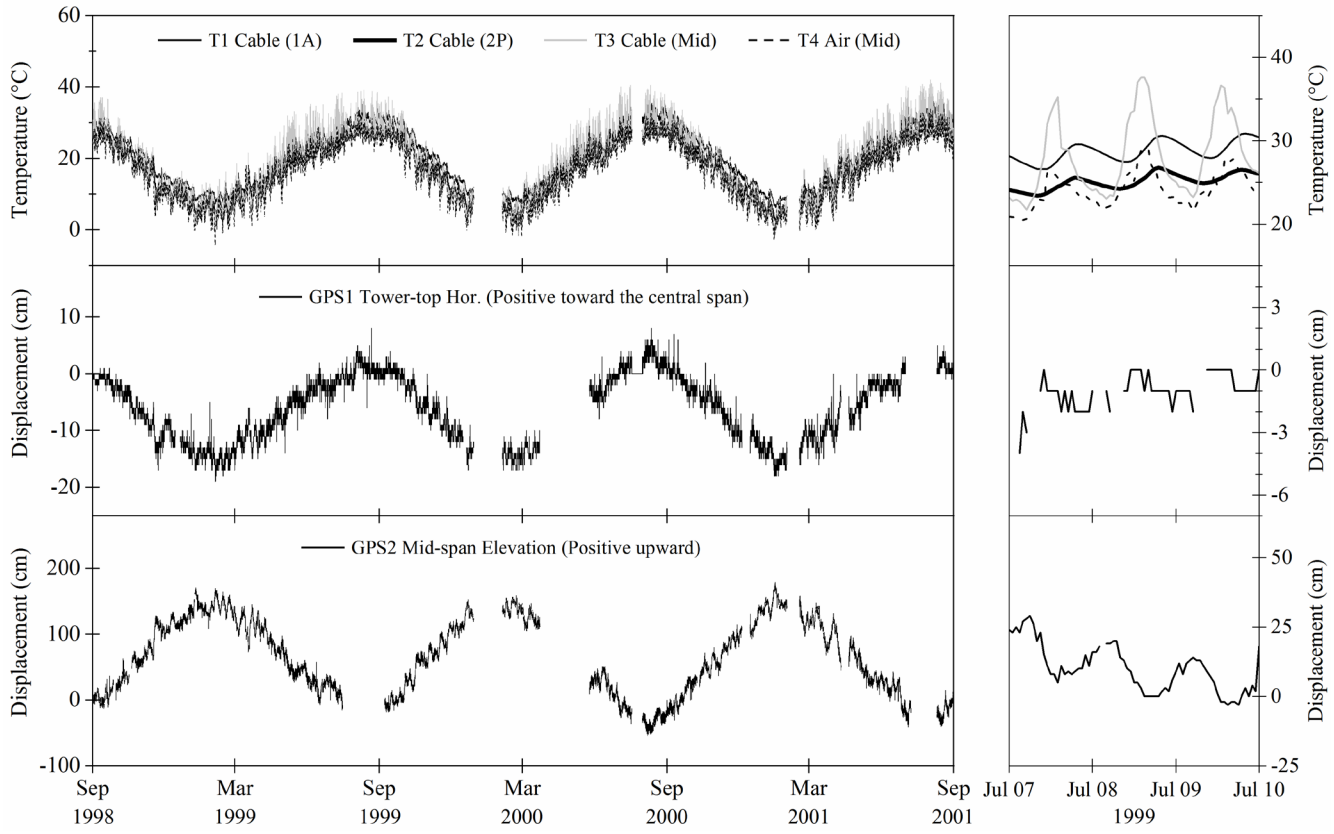

Fig. 3. Temperature and structural displacement measured during 1998–2001.

The mid-span vertical displacement of the main cable versus the cable temperature is plotted in Fig. 4, which shows a linear relation. The slope of the linear regression equation (dashed line) is calculated as $-0.0701\,\text{m}/^{\circ}\text{C}$, indicating that the mid-span elevation decreases by 0.0701 m, with a unit increase in cable temperature. A similar linear regression analysis shows that the tower top moves 0.0069 m toward the main span, with a unit increase in cable temperature.

The temperature-induced displacement of the bridge is calculated using the formulas provided herein. From Eqs. (16) and (17), when the cable temperature increases by 1°C, the elevation of the main cable at the mid-span decreases by 0.0708 m and the tower top moves 0.0074 m toward the main span. Therefore, the results obtained using the derived formulas agree well with the field measurement data. The calculation is based on the following parameters: (1) $l_1 = 959.999\,\text{m}$, $l_2 = 1990.796\,\text{m}$, and $l_3 = 960.295\,\text{m}$; (2) $n_1 = 0.046$, $n_2 = 0.098$, and $n_3 = 0.046$; (3) $\alpha_1 = 14.326^{\circ}$, $\alpha_2 = -0.008^{\circ}$, and $\alpha_3 = -14.300^{\circ}$; (4) $h_{P1} = h_{P2} = 287.200\,\text{m}$; (5) $\theta_C = \theta_P = 1.2\times10^{-5}\,^{\circ}\text{C}^{-1}$; and (6) $\delta T_C = \delta T_P = 1\,^{\circ}\text{C}$. The calculated results are also shown in Fig. 4 (solid lines passing the center of the data points).

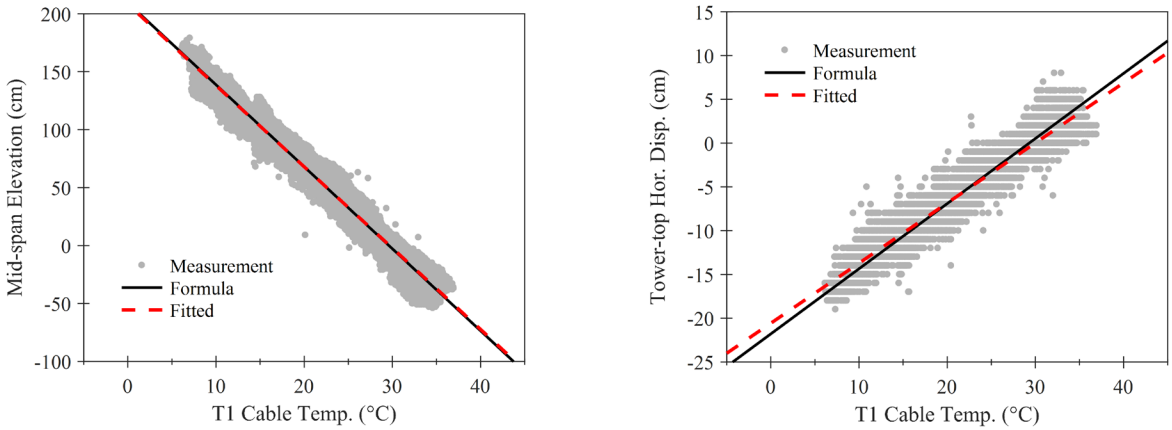

(a) T1 versus midspan elevation.

(b) T1 versus tower-top horizontal displacement.

Fig. 4. Structural displacement versus temperature change (1998–2001).

With the simplified Eqs. (28) and (29) and $\delta T_C = \delta T_P = 1\,^\circ\mathrm{C}$, the elevation of the main cable at the mid-span decreases by 0.0715 m, the tower top moves 0.0075 m toward the main span, and both provide good estimates of bridge deformation. Furthermore, when the sag of side-span cables is neglected, the aforementioned two quantities are 0.0865 and 0.0115 m, according to Eq. (31). In this case, neglecting the side-span cable sags leads to considerable errors.

The formulas and simplified formulas are also applied to seven other long-span suspension bridges. Fig. 5 presents δf_2 and δl_i ($i = 1, 2, 3$) of the eight bridges calculated using different formulas, according to the geometric information listed in Table 1. Most of the relative errors of Eqs. (28) and (29) with respect to the exact formulas [Eqs. (16) and (17)] are <2%, indicating the effectiveness of the simplified formulas. The relative errors of Eq. (31) are small for all bridges except the Akashi Kaikyo bridge, which contains a long side span.

In conclusion, Eqs. (28) and (29) present an excellent approximation of Eqs. (16) and (17). Eq. (31) provides a satisfactory estimate of most suspension bridges and fair errors for the Akashi Kaikyo bridge, which has long side spans. The effect of the sag in side-span cables is studied in the following section.

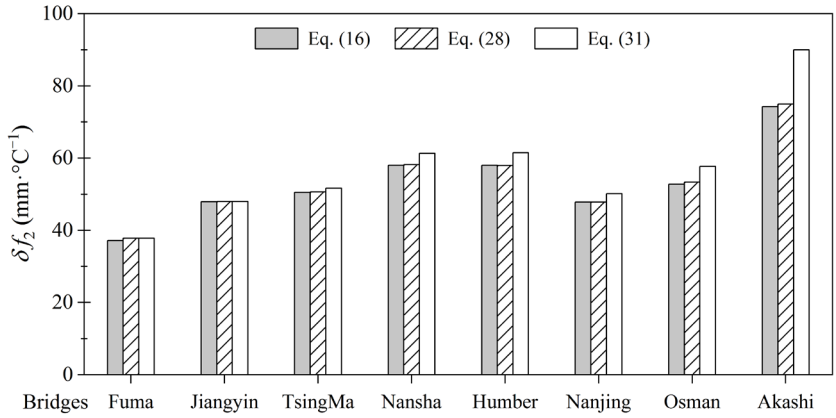

(a) For δf_2.

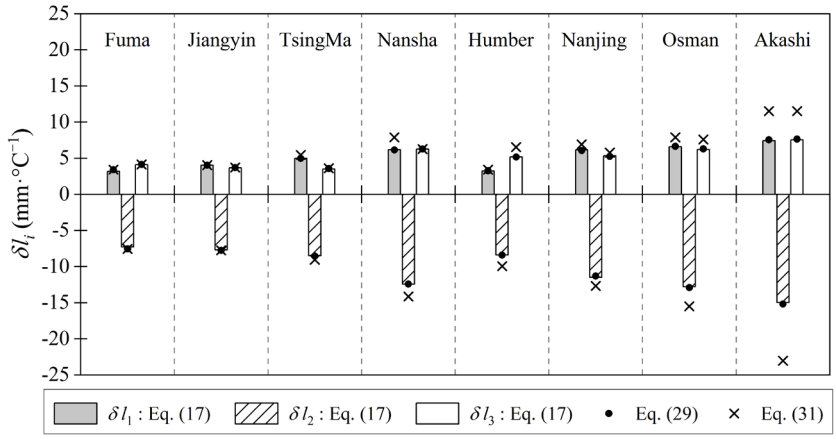

(b) For δl_i ($i = 1, 2, 3$).

Fig. 5. Thermal sensitivity of structural deformations ($\delta T_C = \delta T_P = 1\,^\circ\mathrm{C}$).

Table 1. Geometry of sample bridges.

Bridges	Fuma	Jiangyin	Tsing Ma	Nansha (Nizhou)	Humber	Nanjing No.4	Osman Gazi	Akashi Kaikyo
Location	CHN	CHN	HKG	CHN	GBR	CHN	TUR	JPN
l_1 (m)	285.000	336.506	455.000	658.000	285.000	576.200	658.050	959.999
l_2 (m)	1050.000	1385.042	1377.000	1688.000	1410.000	1418.000	1550.000	1990.796
l_3 (m)	345.000	309.346	300.000	522.000	543.900	481.800	633.250	960.295

Bridges	Fuma	Jiangyin	Tsing Ma	Nansha (Nizhou)	Humber	Nanjing No.4	Osman Gazi	Akashi Kaikyo
Location	CHN	CHN	HKG	CHN	GBR	CHN	TUR	JPN
$\sum_{i=1}^{3} l_i$ (m)	1680.000	2030.894	2132.000	2868.000	2238.900	2476.000	2841.300	3911.090
n_1	0	0	0.024	0.041	0.017	0.032	0.036	0.046
n_2	0.100	0.095	0.093	0.105	0.082	0.111	0.111	0.098
n_3	0	0	0.007	0	0.032	0.028	0.037	0.046
α_1 (°)	25.481	25.670	20.972	18.443	23.901	19.954	19.110	14.326
α_2 (°)	0	0	0	0	0	0	0	-0.008
α_3 (°)	-21.056	-25.789	-27.834	-22.474	-14.088	-23.471	-19.075	-14.300
h_{P1} (m)	213.500	191.236	204.400	256.939	155.500	227.200	241.850	287.200
h_{P2} (m)	169.570	191.236	204.400	256.939	155.500	227.200	241.850	287.200
θ_C (10^{-5}°C^{-1})	1.20	1.20	1.20	1.20	1.20	1.20	1.20	1.20
θ_P (10^{-5}°C^{-1})	1.00	1.00	1.00	1.00	1.00	1.00	1.20	1.20
z_1 (m)	0	0	1.215	5.317	0.348	2.803	4.063	10.331
z_2 (m)	56.000	66.997	63.279	99.748	50.460	93.300	101.404	101.572
z_3 (m)	0	0	0.053	0	2.725	1.752	4.234	10.084
$\sum_{i=1}^{3} z_i$ (m)	56.000	66.997	64.548	105.065	53.533	97.855	109.701	121.987

5 Sag effect of side-span cables

5.1 Side-span cables without suspenders

For side-span cables without hanging a girder, the vertical load q_i ($i = 1, 3$) is the self-weight of cables and is thus much smaller than that of main-span cables. From Eq. (1), the sag of the side-span cables is negligible and Eq. (31) is valid.

5.2 Side-span cables with suspenders

For side-span cables hanging a girder, Eq. (23) shows that $n_i = n_2\zeta_i$ ($i = 1, 3$). To demonstrate the side-span cable sag effect on δf_2, Eq. (28) can be rewritten as

$$\delta f_2 = \frac{z_2}{\sum_{j=1}^{3} z_j} \cdot \frac{3L\theta_C \cdot \delta T_C}{16 n_2 \cos^2 \alpha_2} \tag{32}$$

The sag effect of the side-span cables is represented by a coefficient $\beta_{f_2} = z_2 \Big/ \sum_{j=1}^{3} z_j$. In most suspension bridges, tower tops are at the same level, namely $\alpha_2 = 0$, and the two anchorages and the mid-span of the main-span cable are located at similar elevation level, namely $|h_i| \approx f_2$ ($i = 1, 3$). Therefore, $\cos^2 \alpha_i$ ($i = 1, 3$) can be approximated as

$$\cos^2 \alpha_i = \frac{l_i^2}{l_i^2 + h_i^2} = \frac{l_i^2}{l_i^2 + f_2^2} = \frac{l_i^2}{l_i^2 + n_2^2 \cdot l_2^2} = \frac{\zeta_i^2}{\zeta_i^2 + n_2^2} \tag{33}$$

Using Eq. (33) and $\alpha_2 = 0$, β_{f_2} can be quantified as follows:

$$\beta_{f_2} = \frac{z_2}{\sum_{j=1}^{3} z_j} = \frac{l_2 n_2^2 \cos^2 \alpha_2}{\sum_{j=1}^{3} l_i n_i^2 \cos^2 \alpha_i} = \frac{1}{\frac{\zeta_1^5}{\zeta_1^2 + n_2^2} + 1 + \frac{\zeta_3^5}{\zeta_3^2 + n_2^2}} \tag{34}$$

Fig. 6 presents the relationship between β_{f_2} and ζ_1 for the case of $\zeta_1 = \zeta_3$ and $n_2 = 1/10$. For the Akashi Kaikyo bridge with $\zeta_1 = \zeta_3 = 0.48$, the calculated β_{f_2} value is 0.83, indicating that Eq. (31) presents only 83% of the value calculated with Eq. (28) and causes 17% error. When $\zeta_i < 0.30$ ($i = 1, 3$), which is the case for most long-span suspension bridges, $\beta_{f_2} > 0.95$ and Eq. (31) gives <5% error in the calculation of mid-span displacement. This is observed in Fig. 5 (a) for other seven long-span suspension bridges.

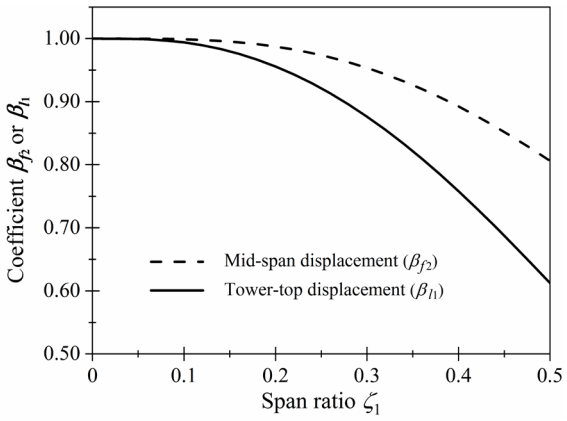

Fig. 6. Influence of side-to-main span ratio on mid-span vertical and tower-top horizontal movements.

Subsequently, the sag effect of side-span cables on the tower-top horizontal displacement is investigated. Because $\delta l_2 = -(\delta l_1 + \delta l_3)$, we only discuss δl_i ($i = 1, 3$). According to Eqs. (29) and (31), a term $\beta_{l_i} = 1 - \left(z_i \Big/ \sum_{j=1}^{3} z_j\right) L / l_i$ ($i = 1, 3$) is introduced. By using the span ratio ζ_i, the total distance L between anchorages can be obtained:

$$L = \left(l_1 + \frac{l_1}{\zeta_1} + \frac{\zeta_3}{\zeta_1} l_1 \right) \tag{35}$$

Assuming $\zeta_1 = \zeta_3$ and $z_1 = z_3$, β_{l_1} can be quantified as

$$\beta_{l_1} = 1 - \frac{z_1}{\sum_{j=1}^{3} z_j} \cdot \frac{L}{l_1} = 1 - \frac{\zeta_1^4}{\zeta_1^2 + n_2^2 + 2\zeta_1^5}(2\zeta_1 + 1) \tag{36}$$

Fig. 6 presents the relation between ζ_1 and β_{l_1}. The sag of side-span cables exhibits more influence on the tower-top horizontal displacement than on the mid-span vertical displacement. For the Akashi Kaikyo bridge with $\zeta_1 = \zeta_3 = 0.48$, β_{l_1} is 0.64. Thus, Eq. (31) causes 36% error. When the two side-span ratios have $\zeta_i = 0.30$ ($i = 1, 3$), Eq. (31) leads to 15% error in the calculation of the tower-top displacement.

The sag effect of the side-span cables is quantified by the modification coefficients, and the results in Ref. [18] correspond to $\beta_{f_2} = \beta_{l_1} = 1.0$. Except for the idealized situation of straight anchor cables (equivalent to $\zeta_1 = 0$ in Fig. 6), both β_{f_2} and β_{l_1} are less than 1.0, which indicates that the sags of side-span cables reduce mid-span vertical and tower-top horizontal displacements. Meanwhile, as $\beta_{f_2} > \beta_{l_1}$, the temperature-induced tower-top movement is more sensitive than the main-span cable sag changes to the sag of side-span cables.

6 Discussions

6.1 Comparison of thermal deformation

The temperature-induced displacement of different components can be compared using the proposed formulas. For the simplified case ($f_1 = f_3 = 0$, $\alpha_2 = 0$, $h_{P1} \approx h_1$, $h_{P2} \approx |h_3|$, $\theta_C \cdot \delta T_C \approx \theta_P \cdot \delta T_P$), the magnitude ratio of δf_i and δl_i ($i = 1, 2, 3$) is identical to the ratio of L_E, which is presented in Eq. (31). Because $n_2 \approx 1/10$ and the side-to-main span ratio is usually <0.5, δf_2 and δD_2 are much larger than δl_i ($i = 1, 2, 3$). For a bridge with a straight side-span cable and $\zeta_1 = \zeta_3 = 0.5$, $\delta f_2 : \delta l_1 : \delta l_2 : \delta l_3 = 7.5 : 1 : 2 : 1$.

Furthermore, the effects of temperature change in main cables and towers can be separated according to Eqs. (16), (17), and (21). Their effects to δf_2 and δl_1 for the eight bridges are compared in Fig. 7, given $\delta T_C = \delta T_P = 1\,^{\circ}\mathrm{C}$. The main-span cable contributes the most (approximately 65%) to δf_2, the side-span cable contributes the second most (each approximately 20%), and towers contribute the least but with an opposite effect (each approximately −5%).

For the horizontal movement of the tower top (δl_1), the temperature change in the side-span cable on the same side contributes the most (approximately 130%), followed by the tower on the same side (approximately −10% to −30%). The subsequent contribution is from the main-span cable (approximately 0 to −30%), which is followed by the contribution of the other side-span cable (less than −10%), and the opposite tower exhibits little effect.

Fig. 7(b) demonstrates that the temperature changes in the right side-span cable cause the movement of the left tower. This indicates the interaction among different members of suspension bridges, which is caused by the cable tension changes with varying temperature. On the contrary, Ref. [18] investigates the deformation of individual members separately and neglects the interaction.

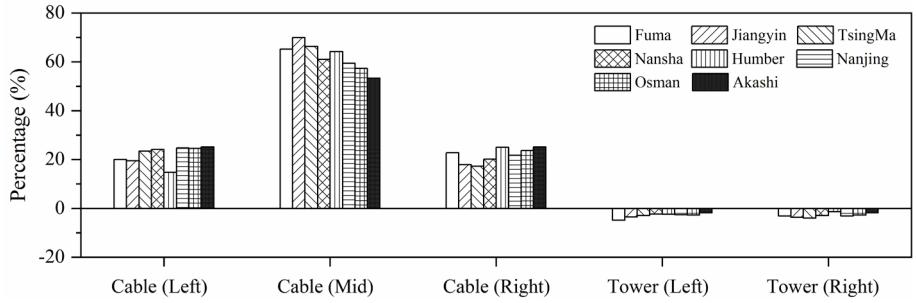

(a) Contribution to the change in the sag of main-span cables.

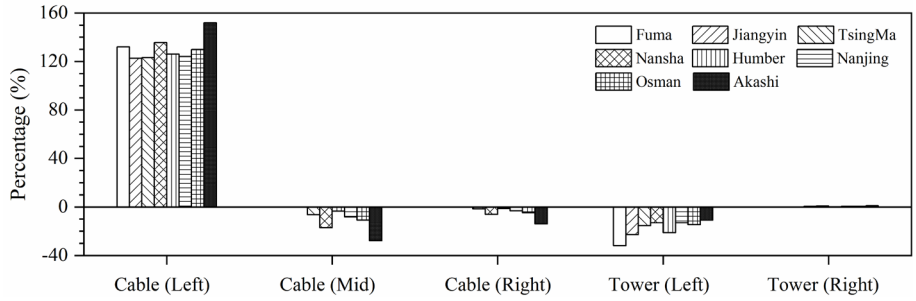

(b) Contribution to left tower-top displacements.

Fig. 7. Contribution of the changes in cable and tower temperatures to structural deformation ($\delta T_{\mathrm{C}} = \delta T_{\mathrm{P}} = 1\,^{\circ}\mathrm{C}$).

6.2 Self-anchored suspension bridges

A self-anchored suspension bridge is a variant of conventional ground-anchored suspension bridges with the main cable anchored on the girder (Fig. 8)[25]. Considering the girder is continuous at the girder–tower intersections with the total length of L_{G}, the distance change between the anchorage points of the main cable can be estimated with $\delta L_{\mathrm{G}} = L_{\mathrm{G}}\theta_{\mathrm{G}} \cdot \delta T_{\mathrm{G}}$, where θ_{G} and δT_{G} are the linear expansion coefficient and temperature change of the girder, respectively. For a two-tower self-anchored suspension bridge, the compatibility condition of all span cables is $\sum_{i=1}^{3} \delta l_i = \delta L_{\mathrm{G}}$. Consequently, the right column vector of Eq. (15) becomes $\begin{bmatrix} Q_1 & Q_2 & Q_3 & 0 & 0 & \delta L_{\mathrm{G}} \end{bmatrix}^{\mathrm{T}}$, and the solution to the new system of equations is given as

$$\delta f_i = \frac{n_i}{\cos\alpha_i} Q_i + \frac{n_i \left(l_i - z_i\right)}{\sum_{k=1}^{3} z_k} \left(-\delta L_{\mathrm{G}} + \sum_{j=1}^{3} \frac{Q_j}{\cos\alpha_j} \right) \tag{37}$$

$$\delta l_i = \frac{Q_i}{\cos\alpha_i} - \frac{z_i}{\sum_{k=1}^{3} z_k} \left(-\delta L_{\mathrm{G}} + \sum_{j=1}^{3} \frac{Q_j}{\cos\alpha_j} \right) \tag{38}$$

From Eq. (38), the change in the girder length δL_{G} is distributed to the change in the span length of each span cable in proportion to the parameter z_i.

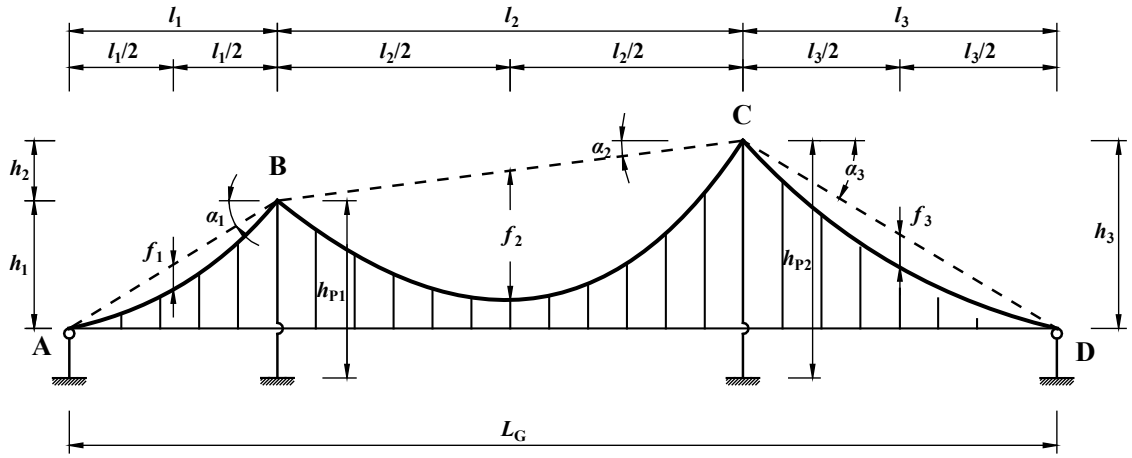

Fig. 8. Self-anchored suspension bridge.

7 Conclusions

In this study, a general analytical formula is proposed for quantifying the thermal deformation of suspension bridges. The main conclusions of the study are as follows:

(1) A simple unified analytical thermal deformation formula with the same form as the 1D thermal expansion formula $L_E\theta_C \cdot \delta T_C$ is derived, where the equivalent length L_E varies for the deformation of different components.

(2) Ignorance of the side-span cables overestimates the global thermal deformation. The sag effect can be characterized by the modification coefficients β_{f_2} and β_{l_1} with $\beta_{f_2} = \beta_{l_1} = 1.0$ corresponding to the results in Ref. [18]. The tower-top movement is more sensitive than the main-span cable sag changes to the sag effect.

(3) For side-span cables with suspenders, the sag effect on the bridge displacement increases with an increase in the span ratio. For most suspension bridges with a span ratio of <0.3, the effect is insignificant; however, for bridges with span ratio of 0.5, the ignorance of side-span cable sags cause 20% and 40% errors for δf_2 and δl_1.

(4) The thermal deformation of the main- and side-span cables and towers is found to interact with each other as a result of the cable tension changes with varying temperature. The closed-form solutions are also available for the self-anchored suspension bridges.

The proposed methodology is more advantageous than the widely used regression and FE analyses because it provides a simple, fast, and accurate quantification of temperature-induced displacement. It is more scientifically rigorous and concise than the approach in Ref. [18] because the sag effects of the side-span cables and the temperature-induced cable tension changes are taken into consideration. Moreover, the method can be extended to other cable structures such as transmission lines or cable car systems.

Acknowledgements

This research was supported by the Hong Kong Polytechnic University (Project No. ZE1F), the Hong Kong Scholars Program (Grant No. XJ2018062), and the Interdisciplinary Research Project for Young Teachers of USTB (Fundamental Research Funds for the Central Universities) (Grant No. FRF-IDRY-19-030).

Conflicts of interest

Yi Zhou, Yong Xia, Yozo Fujino, and Kazunori Yamaguchi declare that they have no conflict of interest or financial conflicts to disclose.

Author contributions

Y.Z., Y.F., and Y.X. designed research; Y.Z., Y.F., Y.X., and K.Y. performed research; Y.Z. and K.Y. analyzed data; and Y.Z., Y.X., and Y.F. wrote the paper.

Appendix A

The assumptions presented in Section 2 are practically reasonable.

When the main cable and suspenders of a suspension bridge are substantially lighter than its suspended girder, the main cable is primarily subjected to the vertical loading uniformly distributed along the span, and thus the cable curve approximates a parabola. Moreover, the cable elastic deformation caused by the changes in tension force can be ignored. From the formulas of δf_i and δl_i [Eqs. (16) and (17) in the main text], we obtain

$$\frac{\delta H_i}{H_i}=\frac{\delta l_i}{l_i}-\frac{\delta f_i}{f_i}=-\frac{1}{\sum_{j=1}^{3} z_j}\sum_{j=1}^{3}\left[\frac{\delta S_j}{\cos\alpha_j}-\tan\alpha_j\left(\delta h_{\mathrm{p}j}-\delta h_{\mathrm{p}(j-1)}\right)\right] \tag{A1}$$

For the Akashi Kaikyo bridge, $\delta H_i/H_i=-3.63\times10^{-4}$ when $\delta T_{\mathrm{C}}=\delta T_{\mathrm{P}}=1^{\circ}\mathrm{C}$. Because the elastic elongation of the main-span cable of this bridge is $S_{\mathrm{e}2}=7.04$ m, the cable deformation induced by tension change caused by a unit increase in temperature can be estimated as follows:

$$\delta S_{\mathrm{e}2}=S_{\mathrm{e}2}\times\frac{\delta H_2}{H_2}=-2.57\ \mathrm{mm} \tag{A2}$$

$\delta S_{\mathrm{e}2}$ is nearly one order of magnitude smaller than the unconstrained (or stress-free) thermal elongation of the main-span cable ($\delta S_2=24.48$ mm).

Second, most long-span suspension bridges employ a flexible tower design to maintain a balance between the cable horizontal tensions on both sides of a tower. Therefore, towers are not supposed to resist the longitudinal displacement of main cables [5].

Third, the main cable is considered to dominate the structural global stiffness in the vertical plane, and the contribution of stiffening girders and suspenders as secondary structures is low. Moreover, for a ground-anchored suspension bridge, both the girder average temperature and differential temperature between the top and bottom surfaces of the girder exhibit negligible effects on main cable deformation, as discussed in [18].

Finally, the main cable is always firmly anchored at anchorage blocks on both ends. Furthermore, relative sliding between the main cable and tower-top saddles is not allowed in the operational stage of suspension bridges.

Appendix B

Eq. (15) can be solved as follows.

The coefficient matrix, denoted as $\mathbf{G}$, can be partitioned as a 2-by-2 block matrix with each block being a 3-by-3 submatrix:

$$\mathbf{G}=\left[\begin{array}{ccc:ccc} c_{n1}l_1^{-1} & 0 & 0 & M_1 & 0 & 0 \\ 0 & c_{n2}l_2^{-1} & 0 & 0 & M_2 & 0 \\ 0 & 0 & c_{n3}l_3^{-1} & 0 & 0 & M_3 \\ \hdashline -f_1^{-1} & f_2^{-1} & 0 & l_1^{-1} & -l_2^{-1} & 0 \\ 0 & -f_2^{-1} & f_3^{-1} & 0 & l_2^{-1} & -l_3^{-1} \\ 0 & 0 & 0 & 1 & 1 & 1 \end{array}\right]=\begin{bmatrix} \mathbf{X}_{\mathrm{A}} & \mathbf{X}_{\mathrm{B}} \\ \mathbf{X}_{\mathrm{C}} & \mathbf{X}_{\mathrm{D}} \end{bmatrix} \tag{B1}$$

The inverse of the above block matrix can be expressed as [26]

$$\mathbf{G}^{-1}=\begin{bmatrix} \mathbf{G}_{\mathrm{A}} & \mathbf{G}_{\mathrm{B}} \\ \mathbf{G}_{\mathrm{C}} & \mathbf{G}_{\mathrm{D}} \end{bmatrix}=\begin{bmatrix} \mathbf{X}_{\mathrm{A}}^{-1}+\mathbf{X}_{\mathrm{A}}^{-1}\mathbf{X}_{\mathrm{B}}\left(\mathbf{X}_{\mathrm{D}}-\mathbf{X}_{\mathrm{C}}\mathbf{X}_{\mathrm{A}}^{-1}\mathbf{X}_{\mathrm{B}}\right)^{-1}\mathbf{X}_{\mathrm{C}}\mathbf{X}_{\mathrm{A}}^{-1} & -\mathbf{X}_{\mathrm{A}}^{-1}\mathbf{X}_{\mathrm{B}}\left(\mathbf{X}_{\mathrm{D}}-\mathbf{X}_{\mathrm{C}}\mathbf{X}_{\mathrm{A}}^{-1}\mathbf{X}_{\mathrm{B}}\right)^{-1} \\ -\left(\mathbf{X}_{\mathrm{D}}-\mathbf{X}_{\mathrm{C}}\mathbf{X}_{\mathrm{A}}^{-1}\mathbf{X}_{\mathrm{B}}\right)^{-1}\mathbf{X}_{\mathrm{C}}\mathbf{X}_{\mathrm{A}}^{-1} & \left(\mathbf{X}_{\mathrm{D}}-\mathbf{X}_{\mathrm{C}}\mathbf{X}_{\mathrm{A}}^{-1}\mathbf{X}_{\mathrm{B}}\right)^{-1} \end{bmatrix} \tag{B2}$$

As $\mathbf{X}_{\mathrm{A}}$ and $\mathbf{X}_{\mathrm{B}}$ are diagonal matrices, $\mathbf{X}_{\mathrm{A}}^{-1}$, $\mathbf{X}_{\mathrm{A}}^{-1}\mathbf{X}_{\mathrm{B}}$, and $\mathbf{X}_{\mathrm{C}}\mathbf{X}_{\mathrm{A}}^{-1}$ are obtained as:

$$\mathbf{X}_{\mathrm{A}}^{-1}=diag\left(\left[c_{n1}^{-1}l_1,\ c_{n2}^{-1}l_2,\ c_{n3}^{-1}l_3\right]\right) \tag{B3}$$

$$\mathbf{X}_{\mathrm{A}}^{-1}\mathbf{X}_{\mathrm{B}}=diag\left(\left[c_{n1}^{-1}l_1M_1,\ c_{n2}^{-1}l_2M_2,\ c_{n3}^{-1}l_3M_3\right]\right) \tag{B4}$$

$$\mathbf{X}_{\mathrm{C}}\mathbf{X}_{\mathrm{A}}^{-1}=\begin{bmatrix} -c_{n1}^{-1}n_1^{-1} & c_{n2}^{-1}n_2^{-1} & 0 \\ 0 & -c_{n2}^{-1}n_2^{-1} & c_{n3}^{-1}n_3^{-1} \\ 0 & 0 & 0 \end{bmatrix} \tag{B5}$$

By introducing a variable $\gamma_i=l_i^{-1}+c_{ni}^{-1}n_i^{-1}M_i$ $(i=1,2,3)$, the matrix $\mathbf{G}_{\mathrm{D}}^{-1}=\mathbf{X}_{\mathrm{D}}-\mathbf{X}_{\mathrm{C}}\mathbf{X}_{\mathrm{A}}^{-1}\mathbf{X}_{\mathrm{B}}$ becomes:

$$\mathbf{G}_{\mathrm{D}}^{-1}=\begin{bmatrix} \gamma_1 & -\gamma_2 & 0 \\ 0 & \gamma_2 & -\gamma_3 \\ 1 & 1 & 1 \end{bmatrix} \tag{B6}$$

According to the general formula of 3-by-3 matrix inversion [26], $\mathbf{G}_{\mathrm{D}}$ can be expressed as:

$$\mathbf{G}_{\mathrm{D}}=\begin{bmatrix} \gamma_1^{-1}\left[1-\left(\sum_{k=1}^{3}\gamma_k^{-1}\right)^{-1}\sum_{k=1}^{1}\gamma_k^{-1}\right] & \gamma_1^{-1}\left[1-\left(\sum_{k=1}^{3}\gamma_k^{-1}\right)^{-1}\sum_{k=1}^{2}\gamma_k^{-1}\right] & \gamma_1^{-1}\left(\sum_{k=1}^{3}\gamma_k^{-1}\right)^{-1} \\ -\gamma_2^{-1}\left(\sum_{k=1}^{3}\gamma_k^{-1}\right)^{-1}\sum_{k=1}^{1}\gamma_k^{-1} & \gamma_2^{-1}\left[1-\left(\sum_{k=1}^{3}\gamma_k^{-1}\right)^{-1}\sum_{k=1}^{2}\gamma_k^{-1}\right] & \gamma_2^{-1}\left(\sum_{k=1}^{3}\gamma_k^{-1}\right)^{-1} \\ -\gamma_3^{-1}\left(\sum_{k=1}^{3}\gamma_k^{-1}\right)^{-1}\sum_{k=1}^{1}\gamma_k^{-1} & -\gamma_3^{-1}\left(\sum_{k=1}^{3}\gamma_k^{-1}\right)^{-1}\sum_{k=1}^{2}\gamma_k^{-1} & \gamma_3^{-1}\left(\sum_{k=1}^{3}\gamma_k^{-1}\right)^{-1} \end{bmatrix} \tag{B7}$$

By substituting Eqs. (B3), (B4), (B5), and (B7) into Eq. (B2), we have the explicit expressions of $\mathbf{G}_{\mathrm{A}}$, $\mathbf{G}_{\mathrm{B}}$, and $\mathbf{G}_{\mathrm{C}}$:

$$\mathbf{G}_{\mathrm{A}}=\begin{bmatrix} c_{n1}^{-1}\gamma_1^{-1}\left(1+\frac{l_1-\gamma_1^{-1}}{\sum_{k=1}^{3}\gamma_k^{-1}}\right) & c_{n2}^{-1}n_2^{-1}\gamma_2^{-1}\frac{f_1-n_1\gamma_1^{-1}}{\sum_{k=1}^{3}\gamma_k^{-1}} & c_{n3}^{-1}n_3^{-1}\gamma_3^{-1}\frac{f_1-n_1\gamma_1^{-1}}{\sum_{k=1}^{3}\gamma_k^{-1}} \\ c_{n1}^{-1}n_1^{-1}\gamma_1^{-1}\frac{f_2-n_2\gamma_2^{-1}}{\sum_{k=1}^{3}\gamma_k^{-1}} & c_{n2}^{-1}\gamma_2^{-1}\left(1+\frac{l_2-\gamma_2^{-1}}{\sum_{k=1}^{3}\gamma_k^{-1}}\right) & c_{n3}^{-1}n_3^{-1}\gamma_3^{-1}\frac{f_2-n_2\gamma_2^{-1}}{\sum_{k=1}^{3}\gamma_k^{-1}} \\ c_{n1}^{-1}n_1^{-1}\gamma_1^{-1}\frac{f_3-n_3\gamma_3^{-1}}{\sum_{k=1}^{3}\gamma_k^{-1}} & c_{n2}^{-1}n_2^{-1}\gamma_2^{-1}\frac{f_3-n_3\gamma_3^{-1}}{\sum_{k=1}^{3}\gamma_k^{-1}} & c_{n3}^{-1}\gamma_3^{-1}\left(1+\frac{l_3-\gamma_3^{-1}}{\sum_{k=1}^{3}\gamma_k^{-1}}\right) \end{bmatrix} \tag{B8}$$

$$\mathbf{G}_{\mathrm{B}}=\begin{bmatrix} -\left(f_1-n_1\gamma_1^{-1}\right)\left(1-\dfrac{\sum_{k=1}^{1}\gamma_k^{-1}}{\sum_{k=1}^{3}\gamma_k^{-1}}\right) & -\left(f_1-n_1\gamma_1^{-1}\right)\left(1-\dfrac{\sum_{k=1}^{2}\gamma_k^{-1}}{\sum_{k=1}^{3}\gamma_k^{-1}}\right) & -\dfrac{f_1-n_1\gamma_1^{-1}}{\sum_{k=1}^{3}\gamma_k^{-1}} \\ \left(f_2-n_2\gamma_2^{-1}\right)\dfrac{\sum_{k=1}^{1}\gamma_k^{-1}}{\sum_{k=1}^{3}\gamma_k^{-1}} & -\left(f_2-n_2\gamma_2^{-1}\right)\left(1-\dfrac{\sum_{k=1}^{2}\gamma_k^{-1}}{\sum_{k=1}^{3}\gamma_k^{-1}}\right) & -\dfrac{f_2-n_2\gamma_2^{-1}}{\sum_{k=1}^{3}\gamma_k^{-1}} \\ \left(f_3-n_3\gamma_3^{-1}\right)\dfrac{\sum_{k=1}^{1}\gamma_k^{-1}}{\sum_{k=1}^{3}\gamma_k^{-1}} & \left(f_3-n_3\gamma_3^{-1}\right)\dfrac{\sum_{k=1}^{2}\gamma_k^{-1}}{\sum_{k=1}^{3}\gamma_k^{-1}} & -\dfrac{f_3-n_3\gamma_3^{-1}}{\sum_{k=1}^{3}\gamma_k^{-1}} \end{bmatrix} \tag{B9}$$

$$\mathbf{G}_{\mathrm{C}}=\begin{bmatrix} c_{n1}^{-1}n_1^{-1}\gamma_1^{-1}\left(1-\dfrac{\gamma_1^{-1}}{\sum_{k=1}^{3}\gamma_k^{-1}}\right) & -c_{n2}^{-1}n_2^{-1}\gamma_2^{-1}\dfrac{\gamma_1^{-1}}{\sum_{k=1}^{3}\gamma_k^{-1}} & -c_{n3}^{-1}n_3^{-1}\gamma_3^{-1}\dfrac{\gamma_1^{-1}}{\sum_{k=1}^{3}\gamma_k^{-1}} \\ -c_{n1}^{-1}n_1^{-1}\gamma_1^{-1}\dfrac{\gamma_2^{-1}}{\sum_{k=1}^{3}\gamma_k^{-1}} & c_{n2}^{-1}n_2^{-1}\gamma_2^{-1}\left(1-\dfrac{\gamma_2^{-1}}{\sum_{k=1}^{3}\gamma_k^{-1}}\right) & -c_{n3}^{-1}n_3^{-1}\gamma_3^{-1}\dfrac{\gamma_2^{-1}}{\sum_{k=1}^{3}\gamma_k^{-1}} \\ -c_{n1}^{-1}n_1^{-1}\gamma_1^{-1}\dfrac{\gamma_3^{-1}}{\sum_{k=1}^{3}\gamma_k^{-1}} & -c_{n2}^{-1}n_2^{-1}\gamma_2^{-1}\dfrac{\gamma_3^{-1}}{\sum_{k=1}^{3}\gamma_k^{-1}} & c_{n3}^{-1}n_3^{-1}\gamma_3^{-1}\left(1-\dfrac{\gamma_3^{-1}}{\sum_{k=1}^{3}\gamma_k^{-1}}\right) \end{bmatrix} \tag{B10}$$

If the second order terms of n in c_{li} and $c_{\alpha i}$ ($i=1,2,3$) (Eqs. (7) and (8)) are omitted, we have:

$$\gamma_i=\frac{3}{16l_in_i^2\cos^2\alpha_i} \tag{B11}$$

$$Q_i=\delta S_i-\sin\alpha_i\cdot\left(\delta h_{\mathrm{P}i}-\delta h_{\mathrm{P}(i-1)}\right) \tag{B12}$$

By introducing a new parameter $z_i=\gamma_i^{-1}$, $\mathbf{G}_{\mathrm{A}}$, $\mathbf{G}_{\mathrm{B}}$, $\mathbf{G}_{\mathrm{C}}$, and $\mathbf{G}_{\mathrm{D}}$ can be rewritten as:

$$\mathbf{G}_{\mathrm{A}}=\begin{bmatrix} \dfrac{n_1}{\cos\alpha_1}+\dfrac{n_1(l_1-z_1)}{\cos\alpha_1\sum_{k=1}^{3}z_k} & \dfrac{n_1(l_1-z_1)}{\cos\alpha_2\sum_{k=1}^{3}z_k} & \dfrac{n_1(l_1-z_1)}{\cos\alpha_3\sum_{k=1}^{3}z_k} \\ \dfrac{n_2(l_2-z_2)}{\cos\alpha_1\sum_{k=1}^{3}z_k} & \dfrac{n_2}{\cos\alpha_2}+\dfrac{n_2(l_2-z_2)}{\cos\alpha_2\sum_{k=1}^{3}z_k} & \dfrac{n_2(l_2-z_2)}{\cos\alpha_3\sum_{k=1}^{3}z_k} \\ \dfrac{n_3(l_3-z_3)}{\cos\alpha_1\sum_{k=1}^{3}z_k} & \dfrac{n_3(l_3-z_3)}{\cos\alpha_2\sum_{k=1}^{3}z_k} & \dfrac{n_3}{\cos\alpha_3}+\dfrac{n_3(l_3-z_3)}{\cos\alpha_3\sum_{k=1}^{3}z_k} \end{bmatrix} \tag{B13}$$

$$\mathbf{G}_{\mathrm{B}}=\begin{bmatrix} -n_1(l_1-z_1)\left(1-\dfrac{\sum_{k=1}^{1}z_k}{\sum_{k=1}^{3}z_k}\right) & -n_1(l_1-z_1)\left(1-\dfrac{\sum_{k=1}^{2}z_k}{\sum_{k=1}^{3}z_k}\right) & -\dfrac{n_1(l_1-z_1)}{\sum_{k=1}^{3}z_k} \\ n_2(l_2-z_2)\dfrac{\sum_{k=1}^{1}z_k}{\sum_{k=1}^{3}z_k} & -n_2(l_2-z_2)\left(1-\dfrac{\sum_{k=1}^{2}z_k}{\sum_{k=1}^{3}z_k}\right) & -\dfrac{n_2(l_2-z_2)}{\sum_{k=1}^{3}z_k} \\ n_3(l_3-z_3)\dfrac{\sum_{k=1}^{1}z_k}{\sum_{k=1}^{3}z_k} & n_3(l_3-z_3)\dfrac{\sum_{k=1}^{2}z_k}{\sum_{k=1}^{3}z_k} & -\dfrac{n_3(l_3-z_3)}{\sum_{k=1}^{3}z_k} \end{bmatrix} \tag{B14}$$

$$\mathbf{G}_{\mathrm{C}}=\begin{bmatrix} \dfrac{1}{\cos\alpha_1}\left(1-\dfrac{z_1}{\sum_{k=1}^{3}z_k}\right) & -\dfrac{z_1}{\cos\alpha_2\sum_{k=1}^{3}z_k} & -\dfrac{z_1}{\cos\alpha_3\sum_{k=1}^{3}z_k} \\ -\dfrac{z_2}{\cos\alpha_1\sum_{k=1}^{3}z_k} & \dfrac{1}{\cos\alpha_2}\left(1-\dfrac{z_2}{\sum_{k=1}^{3}z_k}\right) & -\dfrac{z_2}{\cos\alpha_3\sum_{k=1}^{3}z_k} \\ -\dfrac{z_3}{\cos\alpha_1\sum_{k=1}^{3}z_k} & -\dfrac{z_3}{\cos\alpha_2\sum_{k=1}^{3}z_k} & \dfrac{1}{\cos\alpha_3}\left(1-\dfrac{z_3}{\sum_{k=1}^{3}z_k}\right) \end{bmatrix} \tag{B15}$$

$$\mathbf{G}_{\mathrm{D}}=\begin{bmatrix} z_1-z_1\dfrac{\sum_{k=1}^{1}z_k}{\sum_{k=1}^{3}z_k} & z_1-z_1\dfrac{\sum_{k=1}^{2}z_k}{\sum_{k=1}^{3}z_k} & \dfrac{z_1}{\sum_{k=1}^{3}z_k} \\ -z_2\dfrac{\sum_{k=1}^{1}z_k}{\sum_{k=1}^{3}z_k} & z_2-z_2\dfrac{\sum_{k=1}^{2}z_k}{\sum_{k=1}^{3}z_k} & \dfrac{z_2}{\sum_{k=1}^{3}z_k} \\ -z_3\dfrac{\sum_{k=1}^{1}z_k}{\sum_{k=1}^{3}z_k} & -z_3\dfrac{\sum_{k=1}^{2}z_k}{\sum_{k=1}^{3}z_k} & \dfrac{z_3}{\sum_{k=1}^{3}z_k} \end{bmatrix} \tag{B16}$$

The solution to Eq. (15) in the main text is:

$$\begin{bmatrix} \delta f_1 \\ \delta f_2 \\ \delta f_3 \\ \hdashline \delta l_1 \\ \delta l_2 \\ \delta l_3 \end{bmatrix}=\begin{bmatrix} \mathbf{G}_{\mathrm{A}} & \mathbf{G}_{\mathrm{B}} \\ \mathbf{G}_{\mathrm{C}} & \mathbf{G}_{\mathrm{D}} \end{bmatrix}\begin{bmatrix} Q_1 \\ Q_2 \\ Q_3 \\ \hdashline 0 \\ 0 \\ 0 \end{bmatrix}=\begin{bmatrix} \mathbf{G}_{\mathrm{A}} \\ \mathbf{G}_{\mathrm{C}} \end{bmatrix}\begin{bmatrix} Q_1 \\ Q_2 \\ Q_3 \end{bmatrix} \tag{B17}$$

Substituting Eqs. (B12), (B13), and (B15) into Eq. (B17) leads to Eqs. (16) and (17).

References

[1] Gimsing NJ, Georgakis CT. Cable Supported Bridges: Concept and Design. 3rd ed. Chichester, United Kingdom: John Wiley & Sons Ltd, 2012.

[2] Yanev B. Suspension bridges: An overview. In: Alampalli S, Moreau WJ, eds. Inspection, Evaluation and Maintenance of Suspension Bridges. Boca Raton, FL: CRC Press, 2016: 1-50.

[3] Xu YL, Xia Y. Structural Health Monitoring of Long-Span Suspension Bridges. Abingdon, Oxfordshire: Spon Press, 2011.

[4] Brownjohn JMW, Koo K, Scullion A, List D. Operational deformations in long-span bridges. Struct Infrastruct E. 2015; 11(4): 556-574.

[5] Ogihara K. Design and construction of suspension bridges. In: Alampalli S, Moreau WJ, eds. Inspection, Evaluation and Maintenance of Suspension Bridges. Boca Raton, FL: CRC Press, 2016: 51-68.

[6] Boller C. Structural health monitoring—An introduction and definitions. In: Boller C, Chang FK, Fujino Y, eds. Encyclopedia of Structural Health Monitoring. Chichester, United Kingdom: John Wiley & Sons, Ltd., 2009.

[7] Fujino Y, Siringoringo DM, Ikeda Y, Nagayama T, Mizutani T. Research and implementations of structural monitoring for bridges and buildings in Japan. Engineering-PRC. 2019; 5(6): 1093-1119.

[8] Bao Y, Chen Z, Wei S, Xu Y, Tang Z, Li H. The state of the art of data science and engineering in structural health monitoring. Engineering-PRC. 2019; 5(2): 234-242.

[9] Xu YL, Chen B, Ng CL, Wong KY, Chan WY. Monitoring temperature effect on a long suspension bridge. Struct Control Health Monit. 2010; 17(6): 632-653.

[10] Koo KY, Brownjohn JMW, List DI, Cole R. Structural health monitoring of the Tamar suspension bridge. Struct Control Health Monit. 2013; 20(4): 609-625.

[11] Kashima S, Yanaka Y, Suzuki S, Mori K. Monitoring the Akashi Kaikyo Bridge: First experiences. Struct Eng Int. 2001; 11(2): 120-123.

[12] Kromanis R, Kripakaran P. Predicting thermal response of bridges using regression models derived from measurement histories. Comput Struct. 2014;136: 64-77.

[13] Zhou G, Yi T, Chen B, Chen X. Modeling deformation induced by thermal loading using long-term bridge monitoring data. J Perform Constr Fac. 2018; 32(3): 4018011.

[14] Xia Y, Chen B, Zhou X, Xu Y. Field monitoring and numerical analysis of Tsing Ma Suspension Bridge temperature behavior. Struct Control Health Monit. 2013; 20(4): 560-575.

[15] Tome ES, Pimentel M, Figueiras J. Structural response of a concrete cable-stayed bridge under thermal loads. Eng Struct. 2018; 176: 652-672.

[16] Zhou L, Xia Y, Brownjohn JMW, Koo KY. Temperature analysis of a long-span suspension bridge based on field monitoring and numerical simulation. J Bridge Eng. 2016; 21(1): 4015027.

[17] Timoshenko SP, Young HD. Theory of Structures. 2 ed. New York: McGraw-Hill, Inc., 1965.

[18] Zhou Y, Xia Y, Chen B, Fujino Y. Analytical solution to temperature-induced deformation of suspension bridges. Mech Syst Signal Pr. 2020; 139: 106568.

[19] Stavridis LT. A simplified analysis of the behavior of suspension bridges under live load. Struct Eng Mech. 2008; 30(5): 559-576.

[20] Thai H, Choi D. Advanced analysis of multi-span suspension bridges. J Constr Steel Res. 2013; 90: 29-41.

[21] Buonopane SG, Billington DP. Theory and history of suspension bridge design from 1823 to 1940. J Struct Eng. 1993; 119(3): 954-977.

[22] Roeder C. Proposed design method for thermal bridge movements. J Bridge Eng. 2003; 8(1): 12-19.

[23] Ministry of Transport of the People's Republic of China. Specifications for Design of Highway Suspension Bridge. JTG/T D65-05—2015. Beijing: China Communications Press, 2015.

[24] Kitagawa M. Technology of the Akashi Kaikyo Bridge. Struct Control Health Monit. 2004; 11(2): 75-90.

[25] Ochsendorf JA, Billington DP. Self-anchored Suspension Bridges. J Bridge Eng. 1999; 4(3): 151-156.

[26] Bernstein DS. Matrix Mathematics: Theory, Facts, and Formulas. 2nd ed. Princeton, NJ: Princeton University Press, 2009.